



HAL
open science

Drop dynamics of viscoelastic filaments

Hrishikesh Pingulkar, Jorge Peixinho, Olivier Crumeyrolle

► **To cite this version:**

Hrishikesh Pingulkar, Jorge Peixinho, Olivier Crumeyrolle. Drop dynamics of viscoelastic filaments. Physical Review Fluids, 2020, 5 (1), pp.1-8. 10.1103/PhysRevFluids.5.011301 . hal-02533880

HAL Id: hal-02533880


<https://hal.science/hal-02533880>

Submitted on 6 Apr 2020

HAL is a multi-disciplinary open access archive for the deposit and dissemination of scientific research documents, whether they are published or not. The documents may come from teaching and research institutions in France or abroad, or from public or private research centers.

L'archive ouverte pluridisciplinaire **HAL**, est destinée au dépôt et à la diffusion de documents scientifiques de niveau recherche, publiés ou non, émanant des établissements d'enseignement et de recherche français ou étrangers, des laboratoires publics ou privés.

Drop dynamics of viscoelastic filaments

Hrishikesh Pingulkar,¹ Jorge Peixinho ,^{1,2} and Olivier Crumeyrolle¹

¹*Laboratoire Ondes et Milieux Complexes, CNRS and Université Le Havre Normandie,
76600 Le Havre, France*

²*Laboratoire PIMM, CNRS, Arts et Métiers Institute of Technology,
Cnam, HESAM Université, 75013 Paris, France*

The stretching of viscoelastic polymer solutions close to breakup can create attached drops on a filament, whose properties and dynamics are little understood. The stretching of capillary bridges and the consecutive filament, until its breakup, can be quantified using diameter-space-time diagrams, which demonstrate hierarchy, as well as asymmetry of satellite drops around a big central drop. All drops experience migration, oscillation, and merging. In addition, the position of the minimum diameter on the filament is determined, along with the number of drops, their positions, the diameters of drops and the filament breakup time. The maximum number of drops on the filament can be predicted using the Deborah number. The diagrams also quantify the large Hencky strains in the filaments before pinch-off. The obtained minimum diameter is used to measure the extensional viscosity, which indicates the effect of polymer concentration and direction of filament thinning.

Introduction. Understanding the extensional flow properties of polymer solutions is of practical and physical importance for many commercial applications such as spraying, coating, inkjet printing, food processing, atomization, etc. Most of these processes undergo filament breakup of solutions containing dissolved polymers and the extensional viscosity of these solutions plays an important role in the thinning and the drop dynamics. In contrast to Newtonian fluids, which have their extensional viscosity directly proportional to the shear viscosity, the extensional viscosity of viscoelastic fluids is more complex. Macromolecular solutions exhibit large extensional viscosity [1–10] because extensional flows are irrotational and presumably more efficient at disentangling or orienting flexible polymer molecules. It has been known for 50 years [11,12] that capillary jets of viscoelastic polymer solutions exhibit the peculiar morphology called beads on a string (BOAS). The instability and the initial sinusoidal growth has been reported [13–15] and has also been observed in the stretching of capillary bridges using extensional rheometers such as Capillary Breakup Extensional Rheometer (CaBER) [7,16–21]. These studies have consistently evidenced the linear viscous-capillary thinning, the exponential polymeric thinning [22], and the existence of drops attached to a thin filament [2,23–28], depending on the fluid properties.

A remarkable feature of the thinning of viscoelastic solution is the ability to form long and persistent filaments. Scanning electron microscopy observations [29] suggest the extensional flow is heterogeneous, with local variation of polymer concentration and localized pinching [30]. Yet, the BOAS morphology appears from the initial wavelength of capillary instability modified by the central fiber, which behaves as a solid core. The annular film becomes unstable, resulting in drops along the filament. Inside a drop, the polymers are in relaxed state but in the fluid necks, they are in stretched state [29].

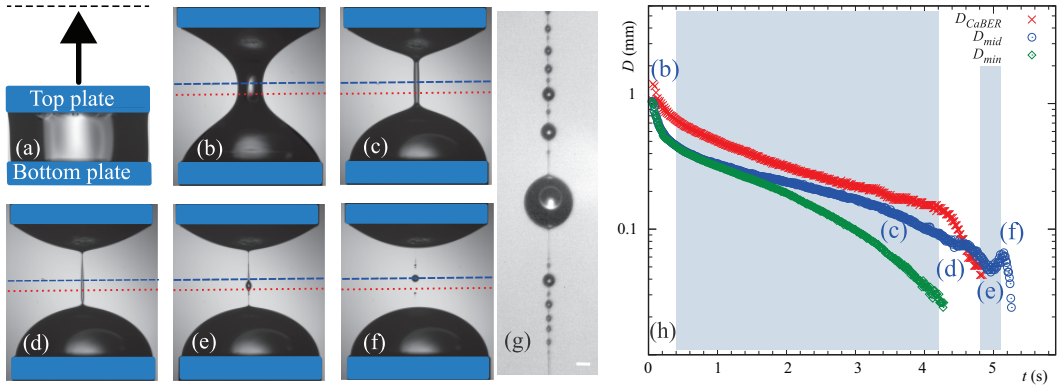


FIG. 1. [(a)–(f)] Photographs of the time evolution of the stretching of a capillary bridge until formation of drops for PEO2000. The fixed midheight position of CaBER’s micrometer is represented as a red dotted line and the midplane position of the filament is represented by a blue dashed line. (g) Enlarged view of BOAS pattern, where the size of the big central drop is $300\ \mu\text{m}$. Scale bar: $100\ \mu\text{m}$. (h) D versus t for PEO2000, measured by the micrometer (red crosses) and by image processing at midplane of the filament, D_{mid} (blue circles), and at the minimum diameter along the filament, D_{min} (green diamonds). The shaded regions [(b)–(f)] represent the different thinning stages corresponding to photographs [(b)–(f)].

From the numerical point of view, the so-called BOAS structure was reproduced using the slender body approximations [31] for Oldroyd-B constitutive equations. The BOAS results as a subtle competition among viscosity, inertia, capillary and viscoelasticity [21] that controls the growth of drops and the pinch-off. The resulting 1D model was used to predict the drop dynamics of the BOAS including drop migration, oscillation, merging, and draining [32]. More recent two-dimensional (2D) axisymmetric simulations, again used the Oldroyd-B model [25,33,34], were able to show the contribution of the polymeric stresses within the filament during the thinning and the drop formation. Specifically, the axial polymeric stress components exhibit a large magnitude and a self-similar radial distribution in time.

Here, a method based on the image analysis is developed, to calculate the extensional viscosity and to map strains. Homologous polymer mixtures or bidisperse polymers at different concentration are tested, covering a large range of dimensionless numbers. For the later stages of filament evolution, a diameter-space-time (DST) diagram is used to represent the drop dynamics.

Experimental setup. To measure the time evolution of the filament diameter, CaBER’s micrometer as well as high-speed image processing have been used to capture the complete filament for measurement of the neck (pinch-off) diameter and midplane diameter. The images are acquired at a rate from 100 to 1000 fps. The camera records stretching, filament thinning, pinch-off, and formation of drops on the filament. More details on the experiment and the protocols are described in the Supplemental Material [35]. Poly-ethylene oxide (PEO), which is a high-molecular-weight polymer, and poly-ethylene glycol (PEG), which has a relatively low molecular weight, are used either separately or in combination with degassed deionized water. The relatively high concentration of PEG, in PEG + PEO solution, makes the solution very dependent on PEG for shear viscosity and on PEO for elasticity. Broadly, our strategy is to control the shear viscosity of solution with PEG and the extensional viscosity with the concentration of PEO, noted c_{PEO} . The molecular weights of PEO and PEG are 8×10^6 and $20\ 000\ \text{g/mol}$, respectively. The solutions properties are in agreement with previous works [36–38].

Figures 1(a)–1(g) depict the time evolution of the filament stretching. Initially, as shown in Fig. 1(a), a liquid bridge of $50\ \mu\text{L}$ volume is formed in between the two plates of CaBER with diameter, $D_0 = 6\ \text{mm}$, separated by the initial height, $L_0 = 2\ \text{mm}$. The top plate is moved upward linearly up to a final height, $L = 6\ \text{mm}$, over the time, $t = 50\ \text{ms}$. Here, $t = 0$ is the instant when

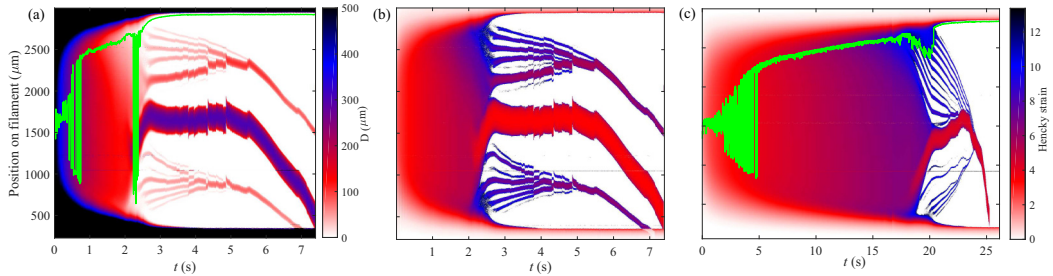


FIG. 2. (a) Diameter-space-time diagram, (b) Hencky strain-space-time diagram for PEO1000, and (c) Hencky strain-space-time diagram for PEG20PEO1000. Here, $t = 0$ is when the separation of the plates of CaBER starts. The green line represents the position of the minimum diameter of the filament.

the top plate starts to move. The formation and thinning of filament until the formation of drops is represented in Figs. 1(b)–1(f). After pinching of the filament at the both ends, the sample solution is pulled toward the center of the filament, termed as recoil [32,39], as shown in Fig. 1(e). The recoiling further develops into drops on a filament, as shown in Fig. 1(f), with an enlarged view of it in Fig. 1(g). From the obtained images, with a self-developed code, the neck diameter or minimum diameter, D_{\min} , and the diameter at filament’s midplane, D_{mid} , are calculated for each image. In Fig. 1(h), the measured diameters are compared. CaBER’s micrometer measures the filament diameter, D_{CaBER} , at the fixed midheight between the plates, whereas, D_{mid} is measured at the midplane of the filament, explaining the shift between the red and blue curves. Clearly, the filament does not have a constant diameter over its length. The D_{mid} curve deviates from D_{mid} from $t = 2$ s. Because of recoiling and coalescence, drops move axially along the thread, respective to midheight and midplane, creating further crests and troughs in the later stages of the diameter versus time plot, as highlighted by the shaded regions (e) and (f) in Fig. 1(h).

Experimental results and discussion. The extension of polymer solution samples up to the breaking of filaments can also be represented through DST diagram and Hencky strain-space-time diagram, as depicted in Fig. 2. The Hencky strain is defined as $\epsilon(z, t) = 2 \ln [D_0/D(z, t)]$, where z is the vertical coordinate. The diagrams are constructed from the images, where the diameter of the filament is converted into a color code, to obtain local diameter in space and time. The diagrams have been obtained for PEO1000 in Figs. 2(a) and 2(b), as well as, for PEG20PEO1000 in Fig. 2(c). The color bars indicate the diameter, D , and the Hencky strain, ϵ , in space and time. It can be observed that for both solutions, a pattern emerges after the thinning of the filament, where the arrangement of drops on the filament proceeds with a relatively large drop forming around the midheight with a diameter of 220–320 μm , accompanied by small drops on both sides. At later time, for PEO solutions in Fig. 2(a), two relatively medium size satellite drops, with diameter varying from 50 to 150 μm , are observed on the either side of the big drop. Interestingly, the diameter of the satellite drop on the top of the big drop is larger than the diameter of the satellite drop on the bottom. The sizes of smaller drops, other than the big drop and two satellite drops, are less than 50 μm . In the case of Hencky strain-space-time diagrams, it can be observed that ϵ is fairly uniform throughout the filament before pinching. After $t = 2.5$ s for PEO1000 and $t = 18$ s for PEG20PEO1000, drops on the filament appear and ϵ is higher in the smaller drops compared to the big central drop. In addition, the position of the minimum diameter, D_{\min} , for each filament is calculated and represented by the green line. D_{\min} is initially located at the midheight and then oscillates in between both ends of the filament. After pinching, D_{\min} is systematically located at the top of the filament, where the breakup occurs, presumably because of gravity effects. From Fig. 2(c), it can be seen that ϵ corresponding to the green line varies significantly over time after pinching. Sudden vertical jumps in the diagrams are observed because of coalescence of small drops, for example, in Fig. 2(a) at $t = 4.3$ and 4.8 s. It suggests an elastic behavior of the filament, as a result

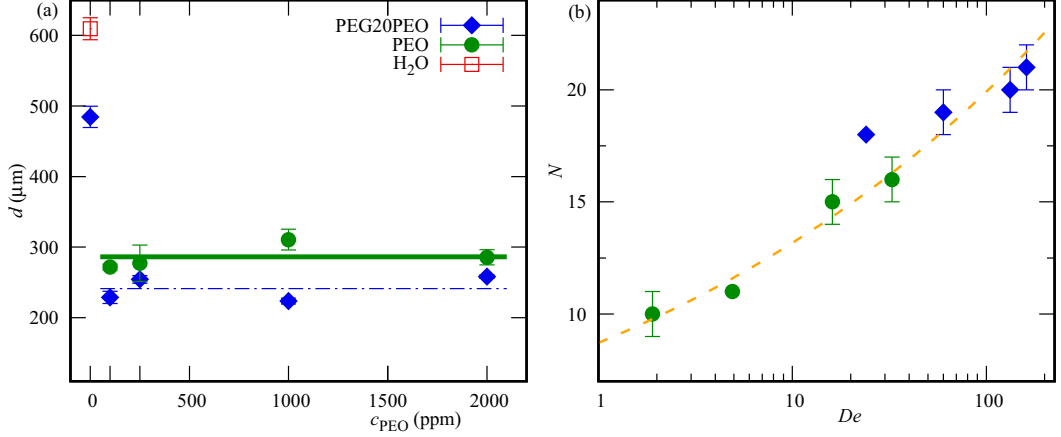


FIG. 3. Summary of the analysis of the diameter-space-time diagrams. (a) Diameter of the final big drop on the filament, d , vs PEO concentration. The thick and the dash-dotted lines represent the average final drop diameter. The error bars indicate the dispersion over three rehearsals. (b) Number of drops at the onset of the instability, N , as a function of De . The dashed line is power law fit with $N \propto De^{0.17}$.

of the tension in the filament relaxing following every coalescence. The motion of the filament occurs in the direction of coalescence. With increase in concentration of polymers, the thinning time, before the appearance of drops, and filament breakup time, which represents the time taken for filament to break, increase. Another feature of DST diagrams is the systematic fall of the big drop toward the bottom. The diagrams allow us to measure the falling of the big drop. From the solution properties and the maximum diameter of the big central drop ($d_{\text{PEG20PEO1000}} = 224 \mu\text{m}$), the calculated weight of the drop is 59.41 nN, assuming spherical shape. At equilibrium condition, the tension in the filament is equal to the weight of the drop. Then, the drop starts to fall. From Fig. 2(c), the equilibrium condition occurs at $t \simeq 24$ s and at $z_0 = 1312 \mu\text{m}$, where z_0 is the vertical position of the drop on the filament from the bottom plate. The falling speed of the drop can then be measured; for PEG20PEO1000, $V_{\text{PEG20PEO1000}} = z_0/\Delta t \simeq 1$ mm/s, where Δt is time taken by the drop to fall into the solution pool on the bottom plate. In comparison, the velocity of the drop in free fall, $\sqrt{2gz_0} = 160$ mm/s, is higher than $V_{\text{PEG20PEO1000}}$. Hence, it can be concluded that there is non-negligible pulling force. Also, it can be observed that the diameters of the drops in PEG + PEO solutions are smaller compared to the drops in PEO solutions. It is interesting to notice that there are more satellite drops above the big drop than below, presumably due to gravity effects. The similar behavior is observed for all PEO and PEG + PEO solutions and the additional diagrams are provided in Ref. [35]. The present space-time diagrams give the accurate measurements of the drop's diameter and Hencky strain, whereas previous works [18,40] are based on the grayscale intensity to indicate relative thickness of the drops or the positions of the drops [13]. Overall, the diagrams represent quantitative descriptions of the drop dynamics studied numerically by Li and Fontelos [32], Ardekani *et al.* [25], and Turkoz *et al.* [33] using initial wave perturbation where filament thinning, drop migration, coalescence, and draining were predicted. Additionally, our experiments indicate the hierarchy and asymmetric distribution of satellite drops for all PEO and PEG + PEO solutions.

Further insights of the drop dynamics from the diagrams can be obtained, as in Fig. 3(a), where the diameters of the final big drops on the filament for water and aqueous solutions of PEG, PEO, and PEG + PEO are presented as a function of c_{PEO} . The error bars represent the dispersion over at least three repetitions of the experiment. For water and for PEG20, the diameters are between 600 and 620 and between 480 and 500 μm , respectively. For the solutions containing PEO, the diameters of big drops decrease further in the range of 220–320 μm . It can also be observed that

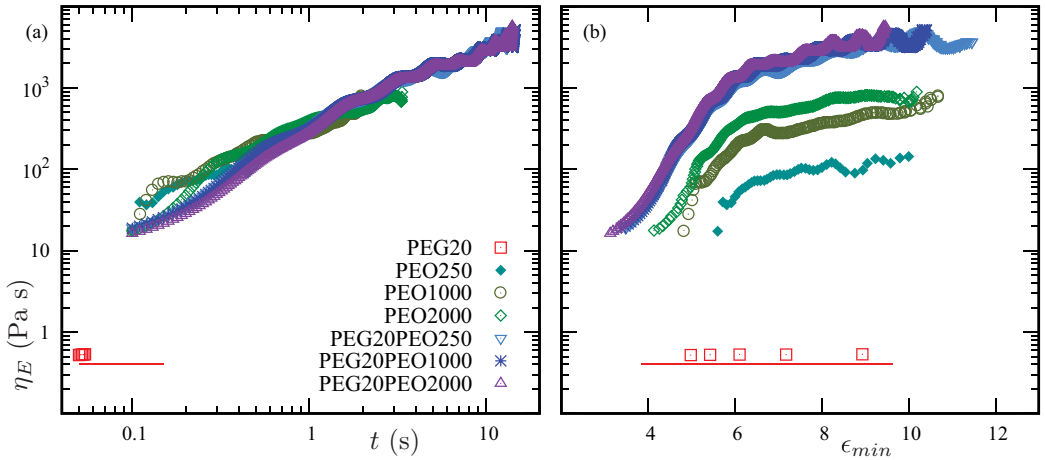


FIG. 4. (a) Extensional viscosity, η_E , for PEG, PEO, and PEG + PEO solutions as a function of time, t . (b) η_E vs Hencky strain, ϵ_{min} , at D_{min} . The red line indicates $\eta_E = 3\eta_0$ for PEG20 from zero shear viscosity measurements.

the average diameter of the big drops for the PEO solutions are comparatively higher than that of the PEG + PEO solutions. However, the size of the big drop remains constant with increase in PEO concentration. In Fig. 3(b), the maximum number of drops on a filament after pinching is plotted against Deborah number, $De = \lambda/\sqrt{\rho D_0^3/8\sigma}$ with λ from CaBER data. The dashed line is a power law fit predicting the maximum number of drops, N , varying as $De^{0.17}$, with the coefficient of determination 0.93. The small value of exponent indicates limited increase in number of drops with De . To the best of our knowledge, there is no theoretical model available to compare this simple scaling law. It is also interesting to note that the number of drops for PEG + PEO solutions is higher than those for PEO solutions for the same c_{PEO} .

To gain more insight into the filament thinning, D_{min} , obtained from DST diagrams, can be used to calculate the apparent extensional viscosity, $\eta_E = -\sigma/(dD_{min}/dt)$, where σ is the surface tension. The obtained results of η_E for PEG, PEO, and PEG + PEO solutions are plotted against time and Hencky strain, $\epsilon_{min} = 2 \ln [D_0/D_{min}(t)]$, in Figs. 4(a) and 4(b), respectively. The figures indicate an increase in η_E with time as well as Hencky strain, in agreement with previous studies [10,42]. Note that at pinching, η_E tends to a constant, which seems to depend on the polymer concentration. A closer look at the Hencky strain-space-time diagrams, for example, Fig. 2(c), retrieves the Hencky strain corresponding to the green line that is ϵ_{min} of Fig. 4(b). From the same figure, it can be seen that all PEG + PEO solutions have comparatively higher η_E than PEO solutions. Hence, with addition of PEG, η_E of PEO solutions increases. Gaillard *et al.* [10] used the same molecular weight of PEG and PEO as well as the minimum diameter of the filament to calculate η_E . Our results give the same η_E for PEG + PEO solutions. In addition, Yu *et al.* [42] used lower molecular weights of PEG and PEO. Hence, they found similar trends but lower values. The change in η_E with filament thinning can be characterized in two distinct regimes. The first regime, where the polymer chains are stretched, corresponds to development of the cylindrical shaped filament in the axial and radial directions. In this regime, for $\epsilon_{min} < 6$, a small increase in ϵ_{min} results in large increase of η_E . Finally, η_E transits to the second regime, where it does not increase much, indicating strain hardening and the fully stretched state of polymers. In this regime, the filament thinning is in the radial direction only.

Relaxation time, λ , is an important factor that quantifies viscoelastic fluids apart from Newtonian fluids. λ is calculated from $D(t)/D_0 \propto \exp(-t/3\lambda)$ [22]. By fitting this equation in the elastocapillary regime, λ is calculated and Fig. 5 represents the change in relaxation time for

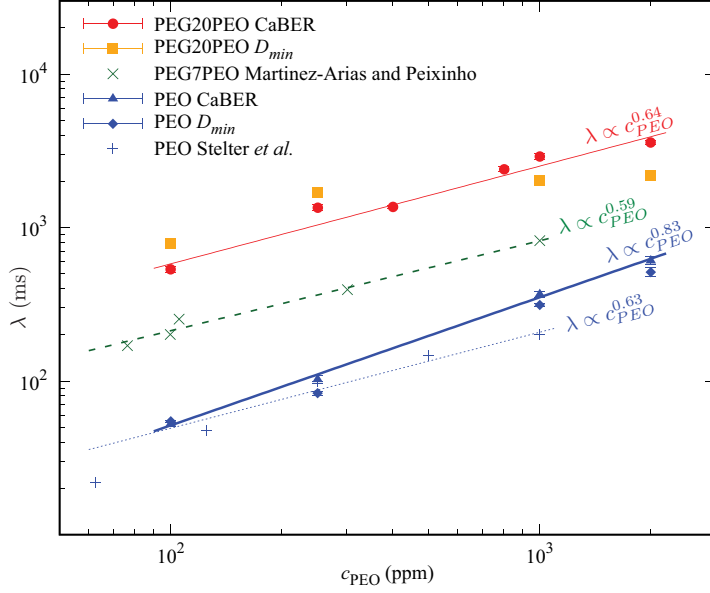


FIG. 5. The relaxation time, λ , as a function of the concentration of PEO, c_{PEO} , for PEO and PEG + PEO solutions. The graph represents comparison of λ calculated by D_{min} obtained from the image processing and from CaBER. Additionally, the lines indicate power law fits. The red thin line is a fit for PEG20PEO solutions and the thick blue line is a fit for PEO solutions. For both fits, λ are measured with CaBER. The dark-green dashed line reproduces the fit of the results of Martínez-Arias and Peixinho [41] for PEG7PEO and the dotted line reproduces the fit of the results of Stelter *et al.* [17] for PEO solutions.

different c_{PEO} for PEG + PEO and PEO solutions on a log-log scale. λ has been calculated using CaBER, as well as D_{min} . λ calculated from D_{min} for PEO solutions is in good agreement with λ from CaBER. It can be seen that λ of PEG + PEO solutions increase with increasing c_{PEO} . Similar trend is observed for PEO solutions. Also, for the same c_{PEO} solutions, λ increases with addition of PEG. For example, relaxation time of PEG20PEO1000 solution is higher compared to the relaxation time of PEO1000 and PEG7PEO1000 solutions. The obtained data are compared with Stelter *et al.* [17] and Martínez-Arias and Peixinho [41]. Both used PEO with molecular weight of 8×10^6 g/mol. The difference in λ measured in the present results and in Ref. [17] can be because of differences in molecular weights of PEO and different protocols in the preparation of solutions. From Fig. 5, for the same c_{PEO} , λ increases with the addition of PEG. For example, the relaxation time of PEG20PEO1000 solution is higher compared to the relaxation time of PEO1000 and PEG7PEO1000 solution. Hence, it can be concluded that higher the concentration of PEG in the aqueous solutions of PEO, the higher will be the relaxation time of the solution.

Conclusions. In conclusion, DST diagrams and the Hencky strain-space-time diagrams presented here allow us to quantify the drop dynamics on the viscoelastic filament. By testing bidisperse polymer solutions of various concentrations, it is found that there is a robust configuration of drops on the filament with a big central drop accompanied by smaller drops on both sides, with systematic movement of the filament in the direction of coalescence. The diagrams also quantify filament thinning, drop migration, coalescence, and draining, together with the position of the minimum diameter. Interestingly, with addition of polymers in water, the size of the big central drop decreases significantly and then remains constant. During the instability, the maximum number of drops increases with De and can be predicted using a power law scaling.

Acknowledgments. The authors thank the Project BIOENGINE, which was cofinanced by the European Union with the European Regional Development Fund and by the Région Normandie. J.P. would like to thank Rodrigue Mbakop for his help with preliminary rheological measurements. Our work also benefited from useful discussions with Prof. Günter Brenn and Prof. Innocent Mutabazi.

- [1] T. Sridhar, V. Tirtaatmadja, D. A. Nguyen, and R. K. Gupta, Measurement of extensional viscosity of polymer solutions, *J. Non-Newt. Fluid Mech.* **40**, 271 (1991).
- [2] J. Dinic, Y. Zhang, L. N. Jimenez, and V. Sharma, Extensional relaxation times of dilute, aqueous polymer solutions, *ACS Macro Lett.* **4**, 804 (2015).
- [3] G. H. McKinley, Visco-elasto-capillary thinning and breakup of complex fluids, in *Annual Rheology Reviews*, edited by D. M. Binding and K. Walters (British Society of Rheology, Wales, UK, 2005), pp. 1–48.
- [4] V. Bergeron, D. Bonn, J.-Y. Martin, and L. Vovelle, Controlling droplet deposition with polymer additives, *Nature (London)* **405**, 772 (2000).
- [5] A. Keller and J. A. Odell, The extensibility of macromolecules in solution: A new focus for macromolecular science, *Colloid Polym. Sci.* **263**, 181 (1985).
- [6] V. Sharma, S. J. Haward, J. Serdy, B. Keshavarz, A. Soderlund, P. Threlfall-Holmes, and G. H. McKinley, The rheology of aqueous solutions of ethyl hydroxy-ethyl cellulose (EHEC) and its hydrophobically modified analogue (hmEHEC): Extensional flow response in capillary break-up, jetting (ROJER) and in a cross-slot extensional rheometer, *Soft Matter* **11**, 3251 (2015).
- [7] L. Campo-Deaño and C. Clasen, The slow retraction method (SRM) for the determination of ultra-short relaxation times in capillary breakup extensional rheometry experiments, *J. Non-Newt. Fluid Mech.* **165**, 1688 (2010).
- [8] G. H. McKinley and T. Sridhar, Filament-stretching rheometry of complex fluids, *Ann. Rev. Fluid Mech.* **34**, 375 (2002).
- [9] C. Clasen, J. P. Plog, W.-M. Kulicke, M. Owens, C. Macosko, L. E. Scriven, M. Verani, and G. H. McKinley, How dilute are dilute solutions in extensional flows? *J. Rheol.* **50**, 849 (2006).
- [10] A. Gaillard, M. Roché, S. Lerouge, C. Gay, L. Lebon, and L. Limat, Viscoelastic liquid curtains: Experimental results on the flow of a falling sheet of polymer solution, *J. Fluid Mech.* **873**, 358 (2019).
- [11] S. Middleman, Stability of a viscoelastic jet, *Chem. Eng. Sci.* **20**, 1037 (1965).
- [12] M. Goldin, J. Yerushalmi, R. Pfeffer, and R. Shinnar, Breakup of a laminar capillary jet of a viscoelastic fluid, *J. Fluid Mech.* **38**, 689 (1969).
- [13] C. Clasen, J. Bico, V. M. Entov, and G. H. McKinley, “Gobbling drops”: The jetting–dripping transition in flows of polymer solutions, *J. Fluid Mech.* **636**, 5 (2009).
- [14] C. Tirel, M.-C. Renoult, C. Dumouchel, D. Lisiecki, O. Crumeyrolle, and I. Mutabazi, Multi-scale analysis of a viscoelastic liquid jet, *J. Non-Newt. Fluid Mech.* **245**, 1 (2017).
- [15] M.-C. Renoult, G. Brenn, G. Pohl, and I. Mutabazi, Weakly nonlinear instability of a Newtonian liquid jet, *J. Fluid Mech.* **856**, 169 (2018).
- [16] M. Stelter, G. Brenn, A. L. Yarin, R. P. Singh, and F. Durst, Validation and application of a novel elongational device for polymer solutions, *J. Rheol.* **44**, 595 (2000).
- [17] M. Stelter, G. Brenn, A. L. Yarin, R. P. Singh, and F. Durst, Investigation of the elongational behavior of polymer solutions by means of an elongational rheometer, *J. Rheol.* **46**, 507 (2002).
- [18] M. S. N. Oliveira and G. H. McKinley, Iterated stretching and multiple beads-on-a-string phenomena in dilute solutions of highly extensible flexible polymers, *Phys. Fluids* **17**, 071704 (2005).
- [19] L. E. Rodd, T. P. Scott, J. J. Cooper-White, and G. H. McKinley, Capillary break-up rheometry of low-viscosity elastic fluids, *Appl. Rheol.* **15**, 12 (2005).
- [20] O. Arnolds, H. Buggisch, D. Sachsenheimer, and N. Willenbacher, Capillary breakup extensional rheometry (CaBER) on semi-dilute and concentrated polyethyleneoxide (PEO) solutions, *Rheol. Acta* **49**, 1207 (2010).

- [21] P. P. Bhat, S. Appathurai, M. T. Harris, M. Pasquali, G. H. McKinley, and O. A. Basaran, Formation of beads-on-a-string structures during break-up of viscoelastic filaments, *Nat. Phys.* **6**, 625 (2010).
- [22] M. I. Kolte and P. Szabo, Capillary thinning of polymeric filaments, *J. Rheol.* **43**, 609 (1999).
- [23] A. L. Shelley and G. H. McKinley, Elasto-capillary thinning and breakup of model elastic liquids, *J. Rheol.* **45**, 115 (2001).
- [24] C. Wagner, Y. Amarouchene, D. Bonn, and J. Eggers, Droplet Detachment and Satellite Bead Formation in Viscoelastic Fluids, *Phys. Rev. Lett.* **95**, 164504 (2005).
- [25] A. M. Ardekani, V. Sharma, and G. H. McKinley, Dynamics of bead formation, filament thinning, and breakup in weakly viscoelastic jets, *J. Fluid Mech.* **665**, 46 (2010).
- [26] M. Aytouna, J. Paredes, N. Shahidzadeh-Bonn, S. Moulinet, C. Wagner, Y. Amarouchene, J. Eggers, and D. Bonn, Drop Formation in Non-Newtonian Fluids, *Phys. Rev. Lett.* **110**, 034501 (2013).
- [27] J. Dinic, L. N. Jimenez, and V. Sharma, Pinch-off dynamics and dripping-onto-substrate (DoS) rheometry of complex fluids, *Lab Chip* **17**, 460 (2017).
- [28] A. Deblais, K. P. Velikov, and D. Bonn, Pearling Instabilities of a Viscoelastic Thread, *Phys. Rev. Lett.* **120**, 194501 (2018).
- [29] R. Sattler, S. Gier, J. Eggers, and C. Wagner, The final stages of capillary break-up of polymer solutions, *Phys. Fluids* **24**, 023101 (2012).
- [30] M. Roché, H. Kellay, and H. A. Stone, Heterogeneity and the Role of Normal Stresses During the Extensional Thinning of Non-Brownian Shear-Thickening Fluids, *Phys. Rev. Lett.* **107**, 134503 (2011).
- [31] D. W. Bousfield, R. Keunings, G. Marrucci, and M. M. Denn, Nonlinear analysis of the surface tension driven breakup of viscoelastic filaments, *J. Non-Newt. Fluid Mech.* **21**, 79 (1986).
- [32] J. Li and M. A. Fontelos, Drop dynamics on the beads-on-a-string structure for viscoelastic jets: A numerical study, *Phys. Fluids* **15**, 922 (2003).
- [33] E. Turkoz, J. M. Lopez-Herrera, J. Eggers, C. B. Arnold, and L. Deike, Axisymmetric simulation of viscoelastic filament thinning with the Oldroyd-B model, *J. Fluid Mech.* **851**, R2 (2018).
- [34] R. Valette, E. Hachem, M. Khalloufi, A. S. Pereira, M. R. Mackley, and S. A. Butler, The effect of viscosity, yield stress, and surface tension on the deformation and breakup profiles of fluid filaments stretched at very high velocities, *J. Non-Newt. Fluid Mech.* **263**, 130 (2019).
- [35] See Supplemental Material at <http://link.aps.org/supplemental/10.1103/PhysRevFluids.5.011301> for (i) the description of the materials and the fluid properties, (ii) space-time diagrams for all the fluids tested, and (iii) two experimental videos for PEG20PEO1000 and PEG20PEO2000 are provided as PEG20PEO1000.gif (the complete filament thinning until breakup) and PEG20PEO2000.avi (the pinching and coalescence).
- [36] Y. Layec and M.-N. Layec-Raphalen, Instability of dilute poly(ethylene-oxide) solutions, *J. Phys. Lett.* **44**, 121 (1983).
- [37] V. Tirtaatmadja, G. H. McKinley, and J. J. Cooper-White, Drop formation and breakup of low viscosity elastic fluids: Effects of molecular weight and concentration, *Phys. Fluids* **18**, 043101 (2006).
- [38] O. Crumeyrolle, N. Latrache, A. Ezersky, and I. Mutabazi, Instability modes observed in a viscoelastic Couette-Taylor flow, *Mech. Ind.* **4**, 397 (2003).
- [39] H. C. Chang, E. A. Demekhin, and E. Kalaidin, Iterated stretching of viscoelastic jets, *Phys. Fluids* **11**, 1717 (1999).
- [40] M. S. N. Oliveira, R. Yeh, and G. H. McKinley, Iterated stretching, extensional rheology, and formation of beads-on-a-string structures in polymer solutions, *J. Non-Newt. Fluid Mech.* **137**, 137 (2006).
- [41] B. Martínez-Arias and J. Peixinho, Torque in Taylor-Couette flow of viscoelastic polymer solutions, *J. Non-Newt. Fluid Mech.* **247**, 221 (2017).
- [42] J. H. Yu, S. V. Fridrikh, and G. C. Rutledge, The role of elasticity in the formation of electrospun fibers, *Polymer* **47**, 4789 (2006).